Migmatization, granite generation and melt accumulation in the Himalayan Orogenic Channel, Central and Eastern Bhutan[†]

A. K. Jain[1,]*, Sushmita[2], Sandeep Singh[2] and P. K. Mukherjee[3,4]

[1]CSIR-Central Building Research Institute, Roorkee 247 667, India
[2]Department of Earth Sciences, Indian Institute of Technology Roorkee, Roorkee 247 667, India
[3]Wadia Institute of Himalayan Geology, Dehra Dun 248 006, India
[4]Present address: Department of Geosciences, Texas Tech University, Lubbock, TX 79409, USA

In Central and Eastern Bhutan Himalaya, the Great Himalayan Sequence (GHS) reveals mesoscopic structures within the migmatite–leucogranite association due to crustal anataxis above the Main Central Thrust (MCT). The first phase of dominant melting generates stromatitic migmatite along the main foliation during high grade of metamorphism, possibly by dehydration melting. Subsequent ductile strike–slip shearing caused *in situ* melting in dilatational sites to produce structureless, non-foliated patchy leucogranite leucosome as well as in boudin necks and post-tectonic patches. In addition, melt-enhanced deformation caused doming of accumulated melt and subsidiary ductile shear zones on either margins of these domes. Surrounded by biotite-rich melanosome, leucosomes destroy the pre-existing foliation during new anatectic phase, which post-dates earlier stromatitic migmatite. These migmatites are the snapshot of mutual relations between newly-developed migmatite and leucogranite melt, and signify the transportation of Himalayan Orogenic Channel to the extreme south in Central and Eastern Bhutan over the Lesser Himalayan sedimentary belt along the MCT.

Keywords: Bhutan, Channel, Himalayan Orogenic migmatite, leucogranite.

MIGMATITE is one of the most exciting mixed association of igneous and metamorphic rocks, which has undergone partial melting (anataxis) during regional metamorphism in orogenic belts[1–3]. It essentially consists of alternating layers of light-coloured mobile melt component phase (the leucosome or neosome), a dark-coloured mafic static residue (the melanosome) and the protolith or host rock – the mesosome (paleosome)[1,3–5]. Such partial melting in orogenic belts provides us insights for deeply-buried crustal processes in the lower crust of the Proterozoic orogens, and in the middle to upper crusts of active orogens like Himalaya, Karakoram and Tibet[6,7].

Extreme mountainous topography of the Himalayas and Karakoram provide us 3D relationships between source rocks, migmatite and melt extraction/segregation into leucogranite bodies whose mutual field relations, structures, petrogenesis and geochronology have been investigated in various studies[8–16]. Two-stage melt generation is recorded at a number of localities in Himalayas, where an earlier main phase of stromatitic migmatite was traversed by subsequent dykes as feeder to the larger leucogranite plutons in upper parts of the Great Himalayan Sequence (GHS)[6]. However, Jain *et al.*[15] record as many as five stages of melting in upper parts of the GHS, Dhauli Ganga valley (Uttarakhand). Partial melting in sillimanite-K-feldspar gneiss produced migmatite and leucogranite containing mus + bio + grt + tur ± crd ± sil ± and, mainly by muscovite dehydration melting in the first stage[2,8], and by subsequent biotite dehydration melting[14].

The outcrops of mesoscopic structures associated with migmatite, described in this study from GHS in Central and Eastern Bhutan, are very explicit in understanding mutual relationships between deformation and various stages of melting of rocks, segregation of melt into migmatite, and their implications for the overall tectonics.

Geological framework

Like the NW and Eastern Himalayas, the Bhutan Himalaya is characterized by distinct longitudinal ENE-trending thrust-bound tectonic belts from south to north (Figure 1). The southernmost Cenozoic Sub-Himalayan (SH) foreland belt mainly of fluvial Neogene-Quaternary Siwalik sequence overrides the Holocene deposits of the Brahmaputra Plains along the Main Frontal Thrust (MFT) and is, in turn, overridden by the Lesser Himalayan (LH) belt along the Main Boundary Thrust (MBT). This belt contains the Neoproterozoic–Early Paleozoic Buxa Group of dolomite, slate and quartzite in the outermost part and the Paleoproterozoic Shumar-Daling Group of quartzite, phyllite-slate and intrusive Mongar granitoids[17]. In the Kuru Chu (valley), the Daling–Shumar Groups contain detrital zircon peak at 1.9–1.8 Ga and other minor peaks
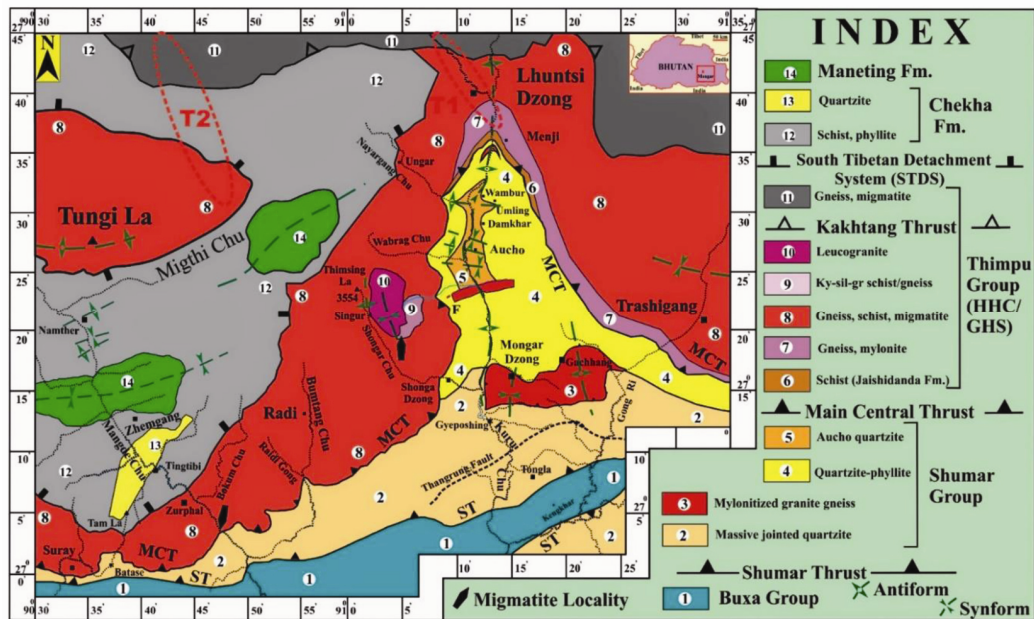
Figure 1. Geological map of Central and Eastern Bhutan Himalaya, showing distribution of the Higher Himalayan Crystallines (HHC)/Great Himalayan Sequence (GHS)/Thimpu Group and migmatite localities under discussion. ST, Shumar Thrust; MCT, Main Central Thrust; KT, Kakhtang Thrust. Compiled after authors' own observations and published maps[17–19,51]. Dashed ellipses indicate locations of Traverse T1 along Kuru Chu and Traverse T2 along Bhumtang sections[24] for pressure, temperature and geochronology data from adjoining regions.
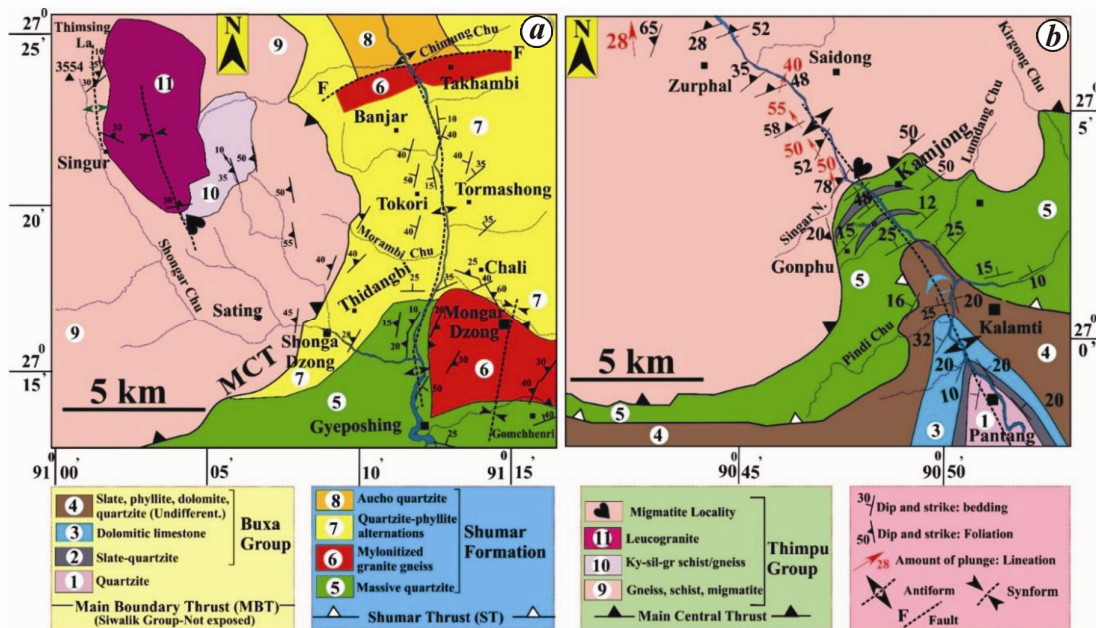

Figure 2. Detailed geological maps of two migmatite localities in the Great Himalayan Sequence (GHS) in the Eastern and Central Bhutan. *a*, Singur locality of migmatite along the Mongar–Thimsing La Road in the uppermost parts of the GHS (Eastern Bhutan). *b*, Mangde Chu locality along the Gonphu–Zurphal Road, washed by the Singar Nadi in immediate vicinity of the MCT (Central Bhutan).

at ~2.5, 2.7 and 3.3 Ga, while associated interstratified metarhyolite has 1.79–1.89 Ga magmatic zircons, thus indicating the depositional age of the Lesser Himalayan sequence to be ~1.90 Ga (refs 18, 19).

The next northern and dominating Great Himalayan Sequence (GHS) belt is thrust over the LH belt along the Main Central Thrust (MCT), and is limited by the South Tibetan Detachment System (STDS) in the north. Migmatite-hosted GHS is remarkable by its V-shaped exposure in the Kuru Chu half-window in Eastern Bhutan (Figure 1). It starts with 30–600 m thick garnet-kyanite-mica schist of the Jaishidanda Formation[17,18,20,21], and many
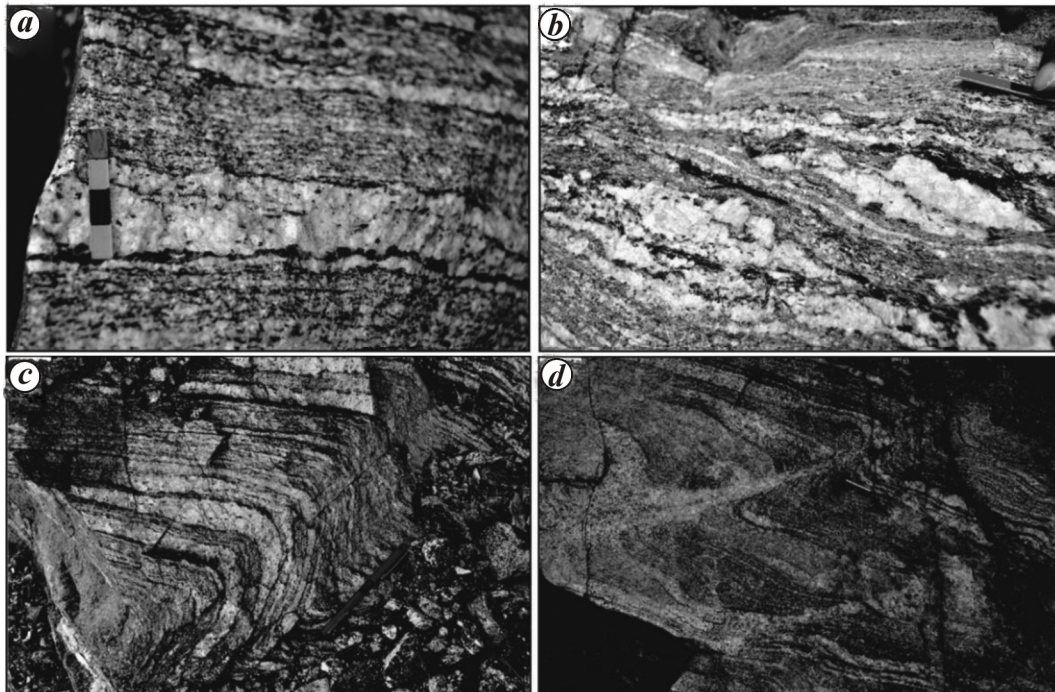
Figure 3. Detailed field characters of migmatite, Singur locality along the Mongar–Thimsing La Road. *a*, Stromatitic migmatite showing dark thin biotite-rich melanosome on either side of foliation-parallel leucosome melt segregation in a band. Mesosome exhibits well-developed original foliation. *b*, Coarse-grained migmatitic gneiss along S-foliation which is sigmoidally bent due to ductile shearing along C-planes, marked by migmatitic layering. *c*, Late stage folding of stromatitic migmatite. *d*, Newly developed leucosome along ductile shear zones, marking axial surfaces of folds.
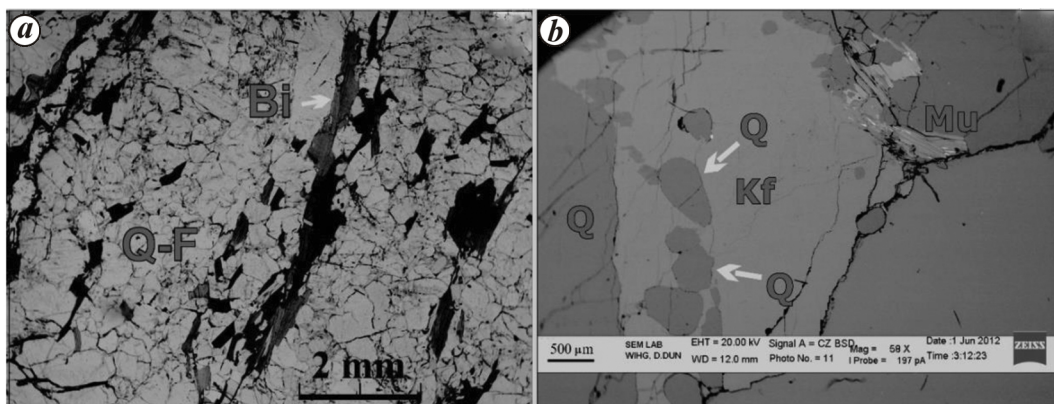
Figure 4. Photomicrographs of gneiss and migmatite from Singur locality. *a*, Gneissosity defined by dark biotite layer (Bi) and thick quartzo-feldspathic leucosome interlayer (Q-F), having randomly orientation mosaic of these minerals. *b*, BSE image showing quartz pseudomorph pods within coarse grained K-feldspars.

km-thick migmatized GHS belt. The latter contains mylonitized granite gneiss at the base, amphibolite-facies kyanite-garnetiferous mica schist and migmatitic gneiss, streaky and porphyroclastic granitic orthogneiss and leucogranite of the Thimphu Group. In the Eastern Bhutan, it exhibits an inverted metamorphic sequence (Figure 1).

An important north-dipping Kakhtang Thrust (KT) separates lower GHS from the still higher grade upper amphibolite facies and more migmatized upper GHS and doubles up the overall thickness of GHS in Bhutan[22–24] (Figure 1). This sequence is overlain by isolated synfor-mal klippe of low-grade metamorphosed late Proterozoic Chekha and Maneting formations of the Tethyan Himalayan Sequence (THS) bound by STDS[17,18,25,26] along the lower contact.

Migmatite localities

Two migmatite localities are described in this work: locality (a) covers the uppermost part of GHS near Singur village along the Mongar-Shonga Dzong-Thimsing La Road at 27°19′42″N : 91°4′23″E (Figures 1 and 2 *a*).
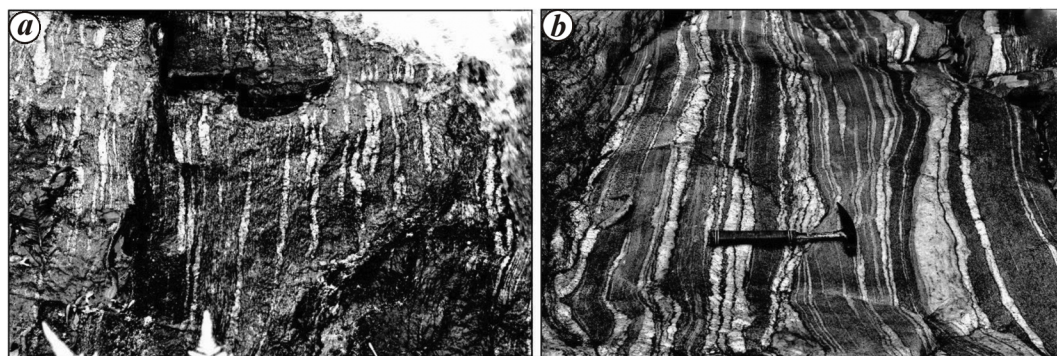
Figure 5. *a*, Exposure along the Mangde Chu River showing alternating mesosome (dark) and leucosome (light) stromatitic migmatite along dip section of main foliation. Near-vertical exposure is observed along a rivulet with water. Width of photo: ~5 m. *b*, Downstream of the same rivulet where near-horizontal main stromatite exposure occurs. Hammer trends across strike of migmatite with its head along direction of dip towards NE. Note ductile dextral shear zone at hammer head.
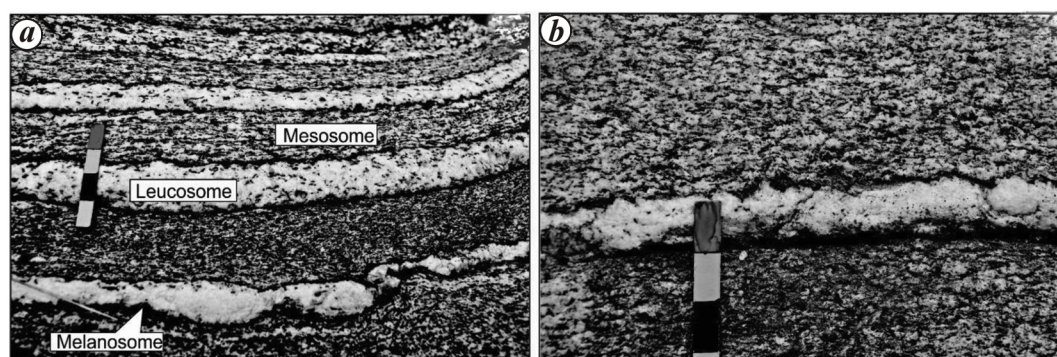
Figure 6. Typical stromatitic migmatite. *a*, Alternating leucosome–melanosome banded layers along with mesosome; all are parallel to the main foliation S_m in migmatite. Scale: 4 cm. *b*, Enlarged quartz-feldspar leucosome band, marked by biotite-rich melanosome on either side. Note one garnet porphyroblast growing in the melanosome. Scale: 3 cm.

The second locality (b) was found in the lowermost parts of the GHS along the Gonphu-Zurphal road section (Mangde Chu valley) at 27°3′45″N : 90°47′30″E within about 500 m of the MCT on its hanging wall (Figures 1 and 2 *b*).

First locality (a-Singur village)

On the western limb of the Kuru Chu half-window, the Mongar-Thimsing La road section exposes the Palaeoproterozoic massive quartzite and quartzite-phyllite alternations of the Shumar Group, having ~1.85 Ga as the maximum depositional age, and the deformed Mongar granite gneiss intrusive within this group of the Lesser Himalaya[18,19]. The GHS, thrust southwards along MCT, contains enormously-thick non-migmatized garnetiferous mica schist, which imperceptibly grades into the higher grade kyanite – and sillimanite-bearing schist and gneiss, now gradually associated with migmatite in upper parts, up the section, thus exhibiting an inverted metamorphic sequence. These rocks regionally strike ENE–WSW to NNW–SSE and dip moderately 30°–40° towards NW.

Near Singur and before crossing Thimsing La, stromatitic migmatite contains alternating leucosome, mesosome and melanosome, paralleling the main foliation S_m (Figure 3 *a*). Coarse-grained quartz and feldspar-rich foliated migmatite bands become sinuous and are deformed by the ductile S–C shear fabric (Figure 3 *b*). Late-stage tight NW-plunging folds deform the migmatite (Figure 3 *c*), though no new foliation paralleling the axial surfaces is decipherable in this exposure. Occasionally, some newly developed leucosome migrates along the axial surfaces of these folds on stromatitic migmatite (Figure 3 *d*). In one such folded migmatite, leucosome possesses light-coloured veinlets, which run parallel to gneissic foliation with well-preserved patchy residual melanosome in its core. Leucosome bands are surrounded by very thin melanosome around it. Coarse-layered limbs exhibit distinctly separated leucosome layers and their accumulation along the foliation with melanosome phases mainly of biotite schlieren.

In both localities, medium-grained granitic gneiss consists essentially of quartz, K-feldspar, plagioclase, muscovite and biotite, and zircon, monazite, allanite and apatite in accessory phases. Strong preferred oriented
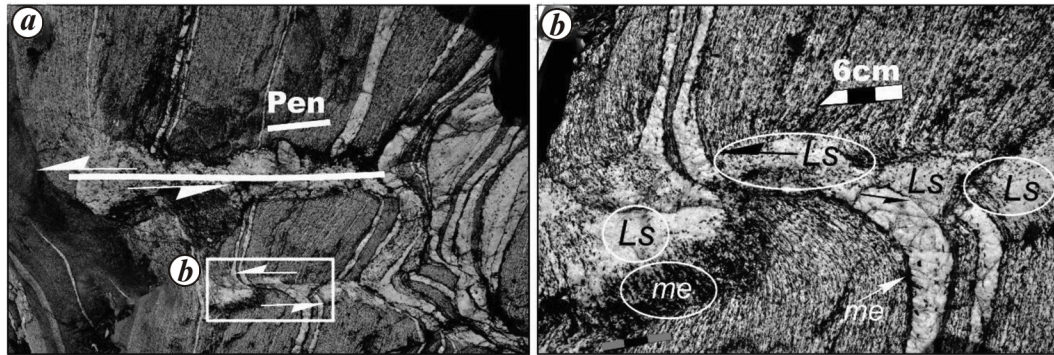
Figure 7. Melting within zones of dilatency along ductile Sinistral Shear Zones (SSZ). *a*, Structureless leucogranite melt in dilatency zones associated with ductile SSZ. Scale: Pen 15 cm. *b*, Enlarged view showing oblique orientation of melt pockets (*Ls*) with respect to average shear direction. Note biotite-rich melanosome (*m*) between leucosome and mesosome. Scale: 6 cm.
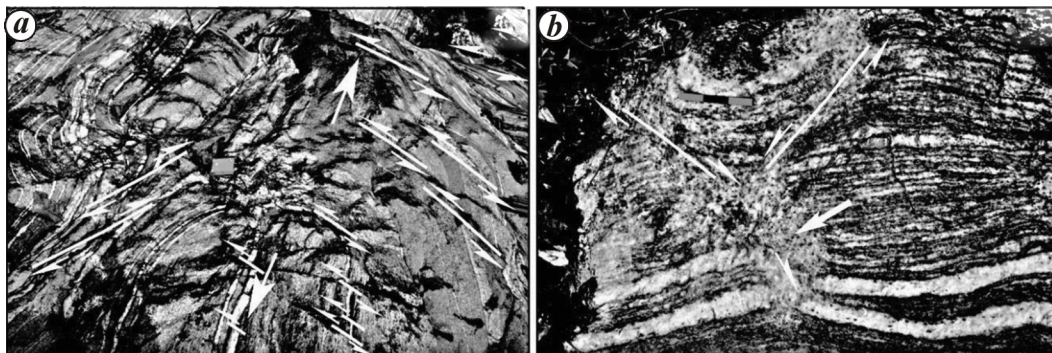
Figure 8. Conjugate ductile shear zones. *a*, Layer-parallel extension due to conjugate set of ductile shear zones and boudin development. Note new leucogranite melt formation in boudin necks (near brunton). Scale: Freiberg brunton. *b*, Boudin necks with massive leucogranite patches (thick yellow arrow). Also note new melt along conjugate shear zones, as well. Scale: 6 cm.

biotite and muscovite flakes alternate with quartzo-feldspathic bands and define well-preserved gneissosity in host rocks (Figure 4 *a*), which are gradually replaced by migmatite.

Melanosome layers are dominated by concentration of biotite and Fe–Ti oxide phases, and are similar to meso-some with many-fold higher biotite and depleted plagio-clase and K-feldspar contents. Plagioclase and quartz are highly ductilely deformed, with chess board extinction in quartz and bent twin lamellae and undulose extinction in plagioclase. Retrograde chlorite and muscovite partially replace biotite. Rounded zircon, monazite, allanite and apatite are frequently observed in the residual melano-some patches as bright grains in BSE images.

In contrast, leucosomes are granitic in composition and much coarser with typical hypidiomorphic-textured quartz, plagioclase and K-feldspar. Randomly oriented undeformed large quartz grains appear in interstitial spaces between coarser K-feldspar and euhedral plagio-clase, as blebs or pod-like inclusion (Figure 4 *b*). Euhedral megacrystic fresh K-feldspar and plagioclase do not show any compositional zoning.

Second locality (Mangde Chu valley)

The second locality (b) was found in lowermost parts of the GHS along the Mangde Chu section above MCT, where Singar Nadi washes these rocks to a polished sur-face. The sequence starts with deformed, foliated and sheared porphyroclastic gneiss, garnetiferous mica schist and associated migmatite, having the same mineral assemblage as described above. The main foliation S_m (gneissosity) in these rocks regionally strikes ENE–WSW in the western parts, almost N–S along the Kuru Chu and trends NNW–SSE on the eastern limb of the Kuru Chu half-window. It dips moderately 30°–40° towards NW and NE on either side of the window.

Close field observations of this locality reveal the following stages of migmatite and leucogranite formation in relation to the various structures.

First stage: stromatitic migmatite: Within 500 m of the MCT zone, ductilely-sheared schist and augen gneiss contain penetrative quartzo-feldspathic concordant leuco-cratic layers to give them a migmatitic appearance
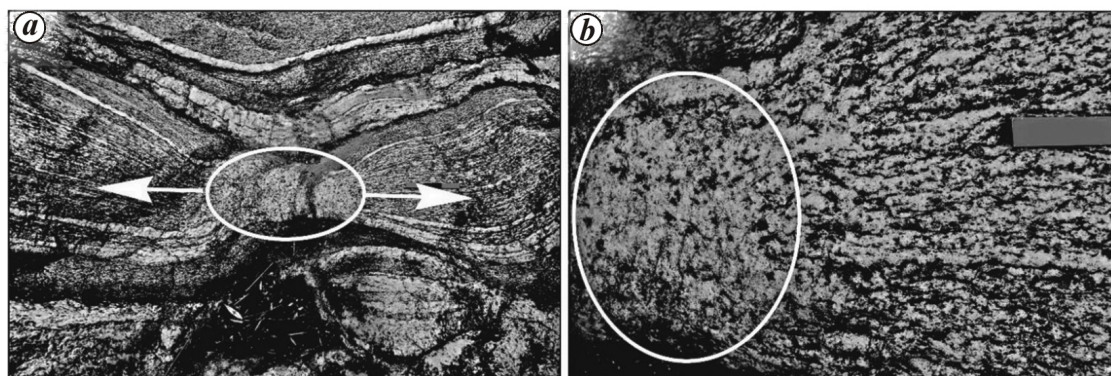
Figure 9. Boudin development and leucogranite. *a*, Typical symmetrical boudin, narrowing of its neck and presence of leucogranite. Scale: 6 cm. *b*, Enlargement of the boudin neck showing destruction of migmatite layering and development of massive leucogranite. Scale: 2 cm.

(Figure 5). It preserves the original pre-partially melted gneissic fabric with centimetre-scale melt segregation, and is well within the domain of metatexite-type on mesoscopic scale[5,27,28]. These stromatitic migmatites are the initial and possibly the earliest stage of occurrences along foliation/gneissosity over which all other migmatite types are developed. In the absence of any other visible planar fabric, it is relatively considered as the oldest structure in the area. Stromatitic migmatite have distinct centimetre-scale banding along S_m foliation, with leucosome and melanosome as physically separable components along well-defined major fabric of regularly-spaced quartz, feldspar and biotite with a few garnet crystals (Figure 6). These leucosome layers alternate with extremely thin smears of biotite-rich melanosome layers along the margins (Figures 3 *a* and 6). Pairs of melanosome–leucosome layers are separated by mesosome layers with less biotite than melanosome layers (Figure 6).

Leucogranite along ductile shear zones: Many small cm-scale leucogranite bodies are observed *in situ* in dilatational sites within the GHS, both along apparent sinistral and dextral ductile shear zones (Figure 7). Non-foliated leucogranite veins/pockets are observed along such shear zones. Such bodies destroy the pre-existing foliation during new anatectic phase, which postdates the earlier stromatitic migmatite (Figure 7 *a*). Stromatitic layers imperceptibly pass into biotite-rich melanosome (*m*) along main foliation, which have the same planar fabric as the stromatitic migmatite[29]. Both of these lose their foliated characters into the adjoining leucogranite patches (*Ls*; Figure 7 *b*)[30].

Leucogranite along boudin necks: One of the important structures at this locality is the development of extensional foliation boudins, and the presence of conjugate shear zones (Figure 8 *a*). Well-foliated stromatitic migmatite layers are, thus, deflected from parallelism to produce classic foliation boudin[29,31]. As a consequence, boudin

necks become narrower and adjoining layers bend (Figure 8 *b*). Thus, these necks become potential dilatational sites for accumulation of leucocratic bodies (Figure 8 *b*).

Deflection of stromatitic layers is observed both along conjugate ductile shear zones (Figure 8 *b*; upper part) and within boudin necks (Figure 8 *b*; central part). Layered migmatite becomes massive by losing its foliated character within boudin neck (Figure 9 *a*), where a true hypidiomorphic biotite-feldspar-quartz assemblage characterizes the undeformed and non-foliated granite (Figure 9 *b*).

Nebulitic leucogranite patches: The last stage of melt accumulation is documented in nebulitic leucogranite as net-like and massive patches on the main foliation S_m, which is totally destroyed within the space now occupied by these patches (Figure 10 *a*). Such a leucogranite patch cross-cuts and deforms the foliation on one side and joins a shear zone on the other; the latter is also occupied by leucocratic melt. In another instance, one such tiny melt patch occurs as a massive leucogranite body where leucosome appears to permeate pervasively into gneissic layering for a while (Figure 10 *b*).

Melt-induced/enhanced deformational structures: At this locality, one exposure of leucogranite melt exhibits typical bulbous character, which resembles 'roof pendant' on a small scale. It is bound by dome and box folds in the melanosome layer, which limits the melt from its migration into the roof – the mesosome part (Figure 11 *a*). A mushroom-shaped body is, thus, created where stromatitic migmatite loses its foliated character into massive leucogranite (Figure 11 *a*). Ductile shear zones, both dextral and sinistral types, develop on either flanks of the bulbous structure (Figure 11 *a* and *d*). The host rock also develops foliated and biotite-rich melanosome, which is folded in the vicinity of melt production site (Figure 11 *b* and *c*). The melanosome layer has its own fabric of biotite flakes and truncates the folded fabric of the mesosome component (Figure 11 *c*).
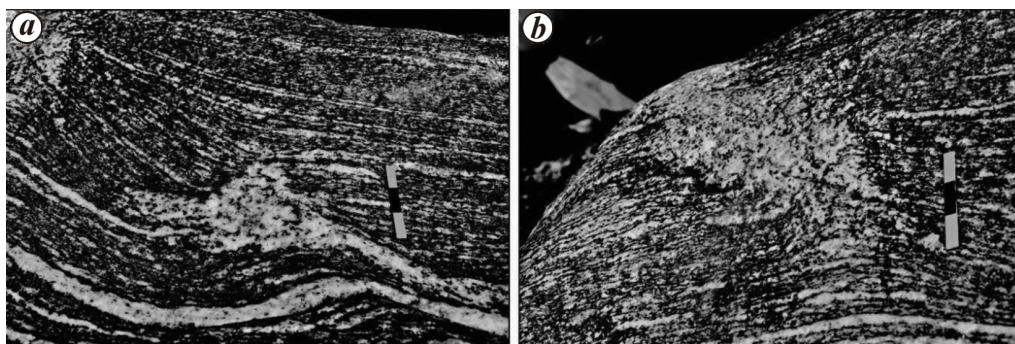
Figure 10. Nebulitic leucogranite patches. *a*, Random distribution of structureless small melt bodies, connected with a shear band in this case. Scale: 3 cm. *b*, Small volume of leucogranite melt pocket, with melt migrating pervasively into the foliation for some distance. Scale: 3 cm.
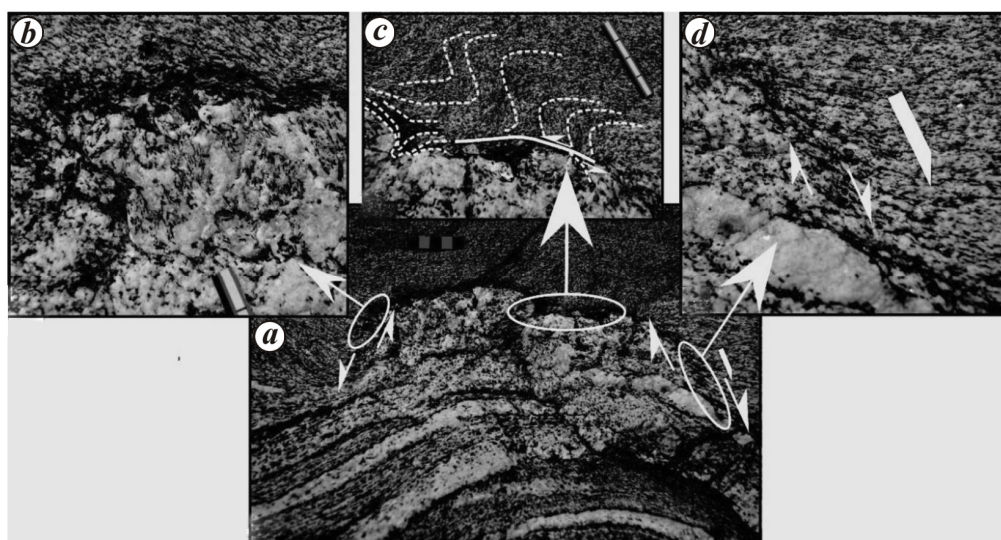
Figure 11. Melt accumulation and associated structures. *a*, Melt-enhanced deformational structures in the Bhutan migmatite. *In situ* leucogranite melt causes localized deformation due to melt-enhanced pressure and development of ductile shear zones on either sides. Scale: 4 cm. *b*, *c*, Dome and box fold along the roof pendant, marked by foliated biotite-rich melanosome layer between leucosome and mesosome. Scale: 1 and 4 cm respectively. *d*, Details of melanosome- rich dextral shear zone along right flank. Scale: Arrow 2 cm.

Discussion

Two localities of migmatite and leucogranite in Central and Eastern Bhutan are associated with parent pelitic biotite gneiss of the Great Himalayan Sequence (GHS). The Mangde Chu migmatite is developed near the base of the GHS within about 500 m of the MCT, while the Singur migmatite is exposed near the top of the sequence. Migmatite and associated leucogranite varieties include: (i) stromatitic migmatite paralleling the main foliation; (ii) leucosome-filled ductile conjugate shear zones; (iii) massive leucogranite patches in dilatational sites of oblique shear zones; (iv) leucogranite bodies along extensional necks of symmetrical foliation boudins, and (v) limbs of folds.

Stromatite migmatite paralleling main foliation contains an association of leucosome with melanosome (restite) along their margins, where these develop parallel to pre-existing foliation of parent biotite gneiss – the mesosome in Central Bhutan (Figures 3 *a* and 6). It suggests *in situ* separation and accumulation of leucosomes, which were produced during dehydration melting. During partial melting, migmatite can be considered as a two-phase system of mechanically weak felsic melt and stronger minerals in restite[32]. As the melt accumulates in pore spaces of pre-existing minerals and expands, it is likely to push unmelted biotite flakes towards margins of layers where these massive concentrates follow foliation and get accumulated along an interphase of another anisotropy, e.g. mesosomes[33]. In this process, the remaining quartz and feldspar gets concentrated. This pattern clearly demonstrates control of an early foliation on melt separation. This migmatite layering can be inferred to be the outcome of melt accumulation and subsequent melt flow. This phenomenon is also supported by lack of any deformational structure within leucogranitic veins[28]. On regional crustal scale, the presence of melanosomes at the margin of melt, all aligned parallel to the earlier foliation,

indicates extraction of melt from these sites or syntectonic melt flow through deforming crust[27,32–36]. On the contrary, such melanosomes may also represent reaction zones between *in situ* melt and host rock[37]. More melts may be drawn from adjoining layers due to variable strain/fluid pressure, thus, a melt-rich layer grows *in situ* by a simple feedback-type mechanism.

Ductile shear zones are the most frequently described structures for granite emplacement and channels for the ascent of magma into low-pressure sites for granite storage[33,38]. Both dextral and sinistral types are most commonly noted near MCT, where many such zones contain small leucogranite bodies (Figures 3 *b*, *d* and 7). When melts are produced in large quantities, their migration may be channelled through such networks of shear zones/dilatant sites through dykes within shear zones (Figure 7 *a*). As melt migrates through such shear zones, these structures deform more rapidly than the surrounding rock[39,40]. Melt starts segregating in dilatational sites or moves through shear zones. Such melt pockets in dilated regions, marked prominently by melanosomes, are also obliquely developed to average orientation of sinistral shear zone in the Bhutanese examples (Figure 7 *b*), indicating that *in situ* melts were possibly generated and filled in the cavities. Alternatively, the melt might have migrated through foliation channels to occupy such cavities. Leucosome-filled conjugate shear bands as well as shear zones paralleling the axial surfaces of folds[41] (Figure 3 *d*) with distinct foliated fabric imply the presence of melt during ductile shearing.

Symmetrical foliation boudins[29,31] are recorded at the Mangde Chu locality where their necks accumulate massive leucosome melt, which lacks any fabric (Figures 8 *b* and 9). As a consequence of this dilatation, foliation of stromatitic migmatite is gradually destroyed in such places, which are favourable sites for *in situ* melting. Alternatively, melt may either migrate or accumulate from adjoining foliated regions in boudin necks. In the latter case, foliation-rich leucosomes should remain preserved in the boudin necks.

Leucosomes of uniform nature, lacking foliations, get accumulated along the pinched necks. Many studies have reported collection of leucosome in boudin necks of deformed migmatites[31,36,38] under plane strain conditions, where dilatency represents an increase in porosity that may enhance the possibility of fluid flow[33,42]. Though generation of leucogranite in boudin necks are visibly observed, such a phenomenon is also demonstrated on large-scale boudinage of the country rocks, causing emplacement of plutons[43].

Partial melting in patches takes place during secondary melting event, where it is randomly generated along triple-junctions of grain boundaries and distributed within the matrix (Figure 10). These melt patches appear to nucleate in tiny massive leucogranite bodies and permeate into the foliation for some distance (Figure 10 *b*). Segregation process first collects the melt to form small isolated melt pockets. As the amount of leucogranite melt is smaller in volume, these remain confined by the strength of the surrounding rocks[44], though these may even deform adjoining host due to enhanced volume (see next section). These lack any fabric within themselves and do not disrupt the pre-existing foliations, hence their secondary *in situ* segregation signifies late-stage crystallization like other cases, described in previous sections.

Melt-enhanced deformation is demonstrated by late-stage undeformed localized accumulation of leucogranite, which is confined by the host gneiss from all sides, acquiring a mushroom-shape body (Figure 11). Since the mushroom is largely massive, melt was not removed and rapidly transported elsewhere. Volume of enhanced melt caused pressure on host migmatite leading to melt-enhanced deformation[32,33,44]. As a consequence, host rock developed both ductile dextral and sinistral shear zones and/or folds of either side of the mushroom in the vicinity of melt production site.

Metamorphic conditions and timing of melting

Though detailed geothermobarometry, mineral assemblages and geochronology of the GHS at these particular localities are beyond scope of this work, it would be worthwhile to assess the available data on *P–T–t* conditions of melting from the adjoining regions in southern Bhutan. In the Kuru Chu valley (Traverse T1, Figure 1), the uppermost garnet-bearing LH sequence yielded *P–T* conditions of 9–13 kb and 650–675°C, while the MCT zone has near 8–10 kb and 650°C, while kyanite-bearing migmatite from GHS has much higher *P–T* conditions of 10–14 kb at 750–800°C (ref. 22).

Detailed U-Pb zircon and monazite dating along this valley (Traverse T1, Figure 1) indicates that peak metamorphism took place at ca. 36–28 Ma in Eastern Bhutan with melt crystallization ca. 27 Ma at structurally highest levels above the Kakhtang Thrust (KT)[24]. Younger leucosome melts crystallized at ca. 16 Ma within the KT zone, and extended until ca. 14–13 Ma in both the KT hanging wall, its footwall, and above the MCT zone. Earlier, U/Pb crystallization ages of monazite and xenotime of 14–15 Ma were recorded from leucogranite and pegmatite along south-verging shear bands, while a thick leucogranite sill is 13.4 ± 0.2 Ma (ref. 22). They inferred that exhumation of MCT zone from 45–35 km to ~18 km occurred from 18–16 to ca. 13 Ma, yielding an average exhumation rate of 3–9 mm per year. In the Central Bhutan (Traverse T2, Figure 1), extended melt crystallization took place from ca. 31 to 19 Ma, while the youngest zircons are similar from either side of KT, indicating its insignificance during underplating of GHS[24]. It is likely that stromatitic migmatite in southern Bhutan, described

herein, were produced during the initial stages of melt crystallization at ca. 27–25 Ma, while subsequent decompression produced massive leucogranite around boudin necks, within shear zones and patches between ca. 16–13 Ma.

Himalayan Orogenic Channel

These migmatite localities, mainly the second locality, signify that GHS metamorphics have undergone extensive transportation along MCT in southernmost parts of Central Bhutan. Structural, metamorphic, leucogranite generation and exhumation within GHS have been modelled within the framework of various tectonic models, e.g. critical wedge[45], ductile shearing[46] and channel flow[47]. The critical wedge model postulates southward extruding metamorphic belt between the non-parallel MCT and STDS at the base and the top respectively[45]. The ductile shear model attempts to interpret consistent top-to-SW ductile shear sense of various kinematic indicators within a broad ductile Higher Himalayan Shear Zone[46,48]. The most popular channel flow model and its different variants visualize either a pure Couette (or linear) flow with simple shear or pure Poiseuille (or parabolic) flow with maximum velocities in its centre or a combination of the two[23,25,49,50].

Within this belt in Eastern Bhutan, leucogranite crystallized at ~27 Ma above the Kakhtang Thrust (KT) and became younger between 25 and 15 Ma within this thrust zone, while still younger leucosome melts extended until ca. 14–13 Ma, both in its hanging wall and footwall above the MCT zone[24]. These melts appeared to have evolved over prolonged period in a southward extruding Himalayan Orogenic Channel, bounded by the coeval MCT at its base and the STDS at the top[48,49].

Conclusions

The presence of garnetiferous migmatite–leucogranite association reveals its genesis within the Himalayan Orogenic Channel with strong structural controls on partial melting, injection and accumulation of generated melt in the GHS in Central and Eastern Bhutan. Stromatitic migmatite containing leucosome, mesosome and melanosome is generated along well-developed foliation during the first stage of partial melting, followed by appearance of structureless, non-foliated and patchy leucogranite-rich leucosomes along subsequent oblique ductile shear zones. Surrounded by biotite-rich melanosome, these obliterate pre-existing foliation during new anatectic phase, which post-dated the earlier stromatitic migmatite.

Comparison with the adjoining region of the GHS indicates that foliation-parallel stromatitic migmatite near Singur village (Locality A) is intimately associated with peak metamorphism around 8–10 kb and 650°C within the MCT zone, with crystallization of the melt ca. 27 Ma

at the structurally highest levels in the upper GHS, and younger melt in massive leucogranite at ca. 14–13 Ma.

1. Brown, M., The definition of metatexis, diatexis and migmatite. *Proc. Geol. Assoc.*, 1973, **84**(4), 371–382.
2. Harris, N. B. W., Ayres, M. and Massey, J., Geochemistry of granitic melts produced during the incongruent melting of muscovite: Implications for the extraction of Himalayan leucogranite magmas. *J. Geophys. Res.*, 1995, **100**, 15767–15777; doi:10.1029/94JB02623.
3. Sawyer, E. W., Atlas of migmatites. *Can. Miner. Spec. Publ.*, 2008, **9**, 386.
4. Mehnert, K. R., *Migmatites and the Origin of Granitic Rocks*, Elsevier Publ. Co, Amsterdam, 1968, p. 405.
5. Wimmenauew, W. and Bryhni, I., Migmatite and related rocks: a proposal on behalf of the IUGS Subcommission on the Systematics of Metamorphic Rocks, 2007, www.bgs.uk/scmr/home.html (web version 1 February 2007).
6. Searle, M. P., Crustal melting, ductile flow, and deformation in mountain belts: Cause and effect relationships. *Lithosphere*, 2013, **5**(6), 547–554; doi:10.1130/RF.L006.1.
7. St-Onge, M. R., Searle, M. P. and Wodicka, N., Trans-Hudson orogen of North America and Himalaya-Karakoram-Tibet orogen of Asia: Structural and thermal characteristics of the lower and upper plates. *Tectonics*, 2006, **25**, TC4006; doi:10.1029/2005TC 001907.
8. Harris, N. and Massey, J., Decompression and anatxis of Himalayan metapelites. *Tectonics*, 1994, **13**(6), 1537–1546; doi:10.1029/94TC01611.
9. Neogi, S., Dasgupta, S. and Fukuoka, M., High P–T polymetamorphism, dehydration melting, and generation of migmatites and granites in the Higher Himalayan Crystalline Complex, Sikkim, India. *J. Petrol.*, 1998, **39**, 61–99.
10. Singh, S., Status of magmatic ages in the Himalaya: a review of geochronological studies. *J. Indian Geophys. Union*, 2001, **5**(1), 57–72.
11. Searle, M. P., Cottle, J. M., Streule, M. J. and Waters, D. J., Crustal melt granites and migmatites along the Himalaya: melt source, segregation, transport and granite emplacement mechanisms. *Earth Environ. Sci. Trans. R. Soc. Edinb.*, 2010, **100**, 219–233.
12. Guo, Z. and Wilson, M., The Himalayan leucogranites: constraints on the nature of their crustal source region and geodynamic setting. *Gondwana Res.*, 2012, **22**(2), 360–376.
13. Imayama, T., Takeshita, T., Yi, K., Cho, D. L., Kitajima, K., Tsutsumi, Y. and Sano, Y., Two-stage partial melting and contrasting cooling history within the Higher Himalayan Crystalline Sequence in the far-eastern Nepal Himalaya. *Lithos*, 2012, **134**, 1–22.
14. Visoná, D., Carosi, R., Montomoli, C., Peruzzo, L. and Tiepolo, M., Miocene andalusite leucogranite in central-east Himalaya (Everest–Masang Kang area): low-pressure melting during heating. *Lithos*, 2012, **144**, 194–208.
15. Jain, A. K., Seth, P., Shreshtha, M., Mukherjee, P. K. and Singh, K., Structurally-controlled melt accumulation: Himalayan migmatites and related deformation, Dhauli Ganga Valley, Garhwal Himalaya. *J. Geol. Soc. India*, 2013, **82**, 313–318.
16. Weinberg, R. F., Himalayan leucogranites and migmatites: nature, timing and duration of anatxis. *J. Metamorph. Geol.*, 2016, doi:10.1111/jmg.12204.
17. Bhargava, O. N., The Bhutan Himalaya: a geological account. *Spec. Publ. Ser. Geol. Surv. India*, Director General, Geological Survey of India, Kolkata, 1995, vol. 39, p. 245.
18. Long, S. and McQuarrie, N. and Tobgay, T., Tectonostratigraphy of the Lesser Himalaya of Bhutan: implications for the along strike stratigraphic continuity of the northern Indian margin. *Geol. Soc. Am. Bull.*, 2011, **123**, 1406–1426; doi:10.1130/B30202.1.
19. McQuarrie, N., Long, S. P. and Tobgay, T., Documenting basin scale, geometry, and provenance through detrital geochemical data: lesson from the Neoproterozoic to Ordovician Lesser,

Greater, and Tethyan Himalayan strata of Bhutan. *Gondwana Res.*, 2013, **23**, 1491–1510; doi:10.1016/j.gr.2012.09.002.

20. Dasgupta, S, Jaishidanda Formation. In *Bhutan Himalaya: A Geological Account* (ed. Bhargava, O. N.), Geol. Surv. India Spec. Publ., Director General, Geological Survey of India, Kolkata, 1995, vol. 39, pp. 79–88.

21. Davidson, C., Grujic, D. E., Hollister, L. S. and Schmid, S. M., Metamorphic reactions related to decompression and synkinematic intrusion of leucogranite, High Himalaya Crystalllines, Bhutan. *J. Metamorph. Geol.*, 1997, **15**(5), 593–612.

22. Daniel, C. G., Hollister, L. S., Parrish, R. R. and Grujic, D., Exhumation of the Main Central Thrust from lower crustal depths, eastern Bhutan Himalaya. *J. Metamorph. Geol.*, 2003, **21**, 317–334; doi:10.1046/j.1525-1314.2003.00445.x.

23. Grujic, D., Hollister, L. S. and Parrish, R. R., Himalayan metamorphic sequence as an orogenic channel: insight from Bhutan. *Earth Planet. Sci. Lett.*, 2002, **198**, 177–191.

24. Zeiger, K., Gordon, S. M., Long, S. P., Kylander-Clark, A. R. C., Agustsson, K. and Penfold, M., Timing and conditions of metamorphism and melt crystallization in Greater Himalayan rocks, eastern and central Bhutan: insight from U–Pb zircon and monazite geochronology and trace-element analyses. *Contrib Mineral. Petrol.*, 2015, **169**, 47; doi:10.1007/s00410-015-1143-6.

25. Grujic, D., Channel flow and continental collision tectonics. In *Channel Flow, Ductile Extrusion and Exhumation in Continental Collision Zones* (eds Law, R. D., Searle, M. P. and Godin, L.), Geol. Soc. Spec. Publ., vol. 268, 2006, pp. 25–37.

26. Yin, A., Cenozoic tectonic evolution of the Himalayan orogen as constrained by along-strike variation of structural geometry, exhumation history, and foreland sedimentation. *Earth-Sci. Rev.*, 2006, **76**, 1–131; doi:10.1016/j.earscirev.2005.05.004.

27. Brown, M., The generation, segregation, ascent and emplacement of granite magma: the migmatite-tocrustally-derived granite connection in thickened orogens. *Earth-Sci. Rev.*, 1994, **36**, 83–130.

28. Brown, M., Averkin, Y. A., McLellan, E. L. and Sawyer, E. W., Melt segregation in migmatites. *J. Geophys. Res.*, 1995, **100**(B8), 15655–15679.

29. Platt, J. P. and Vissers, R. L. M., Extensional structures in anisotropic rocks. *J. Struct. Geol.*, 1980, **2**, 397–410.

30. Jain, A. K., Sushmita and Singh, Sandeep, Photograph of the month. *J. Struct. Geol.*, 2014, **59**, 50.

31. Arslan, A., Passchier, C. W. and Koehn, D., Foliation boudinage. *J. Struct. Geol.*, **30**, 291–309.

32. Davidson, C., Hollister, L. S. and Schmid, S. M., Role of melt during deformation in the deep crust. *Terra Nova*, 1994, **6**, 133–142.

33. Brown, M. and Solar, G. S., Shear-zone systems and melts: feedback relations and self- organization in orogenic belts. *J. Struct. Geol.*, 1997, **20**(2/3), 211–227.

34. Berger, A. and Kalt, A., Structures and melt fractions as indicators of rheology in cordierite- bearing migmatites of the Bayersche Wald (Variscan Belt, Germany). *J. Petrol.*, 1999, **40**, 1699–1719.

35. Brown, M., Orogeny, migmatites and leucogranites: a review. *Earth Planet. Sci. Lett.*, 2001, **110**(4), 313–336.

36. Sawyer, E. W., Melt segregation in the continental crust. *Geology*, 1994, **22**, 1019–1022.

37. Jung, S., Hoernes, S., Masberg, P. and Hoffer, E., The petrogenesis of some migmatites and granites (Central Damara Orogen, Namibia): evidence for disequilibrium melting, wall-rock contamination and crystal fractionation. *J. Petrol.*, 1999, **40**(8), 1241–1269.

38. Brown, M. and Rushmer, T., The role of deformation in the movement of granitic melt: views from the laboratory and the field. In *Deformation-Enhanced Fluid Transport in the Earth's Crust and Mantle* (ed. Holness, M. B.), Chapman & Hall, London, 1997, pp. 111–144.

39. Snoke, A. W., Kalakay, T. J., Quick, J. E. and Sinigoi, S., Deep-crustal shear zone as a result of mafic igneous intrusion in the lower crust, Ivrea-Verbano Zone, Southern Alps, Italy. *Earth Planet. Sci. Lett.*, 1999, **166**, 31–45.

40. Hutton, D. H. W., Depster, T. J., Brown, P. E. and Becker, S. D., A new mechanism of granite emplacement: intrusion in active extensional shear zones. *Nature*, 1990, **343**, 452–455.

41. Vernon, R. H. and Paterson, S. R., Axial-surface leucosomes in anatectic migmatites. *Tectonophysics*, 2001, **335**, 183–192.

42. Ord, A., Mechanical controls on dilatant shear zones. In *Deformation Mechanisms, Rheology and Tectonics* (eds Knipe, R. J. and Rutter, E. H.), Geol. Soc. London Spec. Publ., 1990, **54**, 183–192.

43. D'Eramo, F., Tubía, J. M., Pinotti, L., Vegas, N., Coniglio, J., Demartis, M., Aranguren, A. and Basei, M., Granite emplacement by crustal boudinage: example of the Calmayo and El Hongo plutons (Córdoba, Argentina). *Terra Nova*, 2015, **25**, 423–430.

44. Hollister, L. S. and Crawford, M. L., Melt enhanced deformation: a major tectonic process. *Geology*, 1986, **14**, 558–561.

45. Webb, A. A. G., Yin, A., Harrison, T. M., Célérier, J. and Burgess, W. P., The leading edge of the Greater Himalayan Crystallines revealed in the NW Indian Himalaya: Implications for the evolution of the Himalayan Orogen. *Geology*, 2007, **35**, 955–958; doi:10.1130/G23931A.1.

46. Jain, A. K. and Manickavasagam, R. M., Inverted metamorphism in the intracontinental ductile shear zone during Himalayan collision tectonics. *Geology*, 1993, **21**, 407–410.

47. Beaumont, C., Jamieson, R. A., Nguyen, M. H. and Lee, B., Himalayan tectonics explained by extrusion of a low-viscosity crustal channel coupled to focused surface denudation. *Nature*, 2001, **414**, 738–742.

48. Jain, A. K. and Manickavasagam, R. M., Singh, Sandeep and Mukherjee, S., Himalayan collision zone: new perspectives-its tectonic evolution in a combined ductile shear zone and channel flow model. *Himal. Geol.*, 2005, **26**(1), 1–18.

49. Godin, L., Grujic, D., Law, R. D. and Searle, M. P., Channel flow, ductile extrusion and exhumation in continental collision zones; an introduction. In *Channel Flow, Ductile Extrusion and Exhumation in Continental Collision Zones* (eds Law, R. D., Searle, M. P. and Godin, L.), Geol. Soc. London Spec. Publ., 2006, vol. 268, pp. 1–23.

50. Hollister, L. S. and Grujic, D., Pulsed channel flow in Bhutan. *Geol. Soc. Spec. Publ.*, 2006, **268**, 415–423; doi:10.1144/GSL.SP.2006.268.01.19.

51. Gansser, A., *Geology of the Bhutan Himalaya*, Birkäuser, Basel, 1983, p. 181.